Nawrot, R., et al., 2022, Multiple phyla, one time resolution? Similar time averaging in benthic foraminifera, mollusk, echinoid, crustacean, and otolith fossil assemblages: Geology, v. 50, https://doi.org/10.1130/G49970.1

Geology Supplemental Material

Multiple phyla, one time resolution? Similar time averaging in benthic foraminifera, mollusk, echinoid, crustacean and otolith fossil assemblages

Rafał Nawrot[1], Michaela Berensmeier[1], Ivo Gallmetzer[1], Alexandra Haselmair[1], Adam Tomašových[2], and Martin Zuschin[1]

[1]*Department of Palaeontology, University of Vienna, Althanstrasse 14, Vienna 1090, Austria*

[2]*Earth Science Institute, Slovak Academy of Sciences, Dúbravská cesta 9, Bratislava, 84005, Slovakia*

CONTENTS

SUPPLEMENTARY TEXT ON METHODS

Radiocarbon dating and age calibration

Skeletal elements of foraminifers, echinoids, crustaceans and otoliths were dated by ^{14}C accelerator mass spectrometry (AMS) using the direct carbonate target method (Bush et al., 2013). The ^{14}C-calibrated amino acid racemization (AAR) ages of the two bivalve species sampled from the same core interval were taken from Tomašových et al. (2019), where the details of the AAR calibration procedure can be found. Care was taken to include only skeletal elements that belonged to unique individuals by dating a single element type (right valves of *C. gibba* and left valves of *G. minima*) or by comparing sizes of different elements (e.g., crab dactyli vs. propodi). Regular echinoids were represented in our samples by isolated plates, spines and small test fragments. Thus, we dated only the madreporite, a unique plate in an echinoid test, and analyzed the two regular echinoid species together to maximize sample size. To provide a sufficient amount of material for radiocarbon analysis specimens below 0.20 mg were not considered (all analyzed skeletal elementals were >0.50 mg). All specimens were cleaned by sonicating in water up to several minutes, photographed, measured and weighted.

The samples were processed at the Amino Acid Geochronology Laboratory, Northern Arizona University (NAU), USA and analyzed at the Keck-Carbon Cycle AMS facility, University of California, Irvine, USA. Carbonate targets were prepared with Nb powder following standard protocols described in Bright et al. (2021). Radiocarbon ages were converted to calendar ages using "rcarbon" R package (Crema and Bevan, 2021), Marine20 curve (Heaton et al., 2020) and the regional marine reservoir correction (ΔR) of -61 ± 50 yr for the north-eastern Adriatic Sea (Siani et al., 2001; Tomašových et al., 2019). All ages (including those based on ^{14}C-AAR calibration) are reported here as years before 1950 CE (yr B.P.) and available in Appendix S1.

Age errors associated with AAR dating of bivalve shells exceed age errors in radiocarbon dating, which can inflate estimates of time averaging (Dominguez et al., 2016). As accounting for this effect reduces IQRs of bivalves by several centuries but does not affect the outcome of the analyses (see below and Fig. S1), we used raw AFDs when comparing IQRs among all species. Package "boot" (Canty and Ripley, 2021) was used to calculate 95% bias-corrected bootstrap percentile confidence intervals (also called adjusted percentile intervals) around the IQRs and median ages based on 10,000 resampling iterations. All statistical analyses were done using R 4.1.2 (R Core Team, 2021).

Estimating IQR uncertainty for AAR ages

The estimates of postmortem ages of *Corbula gibba* and *Gouldia minima* were based on medians of posterior distributions estimated by the Bayesian model fitting, following the procedures in Allen et al. (2013). For *C. gibba*, the best-supported calibration (based on 14 shells dated by ^{14}C) is the time-dependent reaction kinetic model for aspartic acid (Asp) D/L, with the initial D/L value estimated from data (TDK1), and lognormal uncertainty, with variance equal to 0.056. The uncertainty of shell age estimates is then defined by random generation of ages on the basis of the lognormal distribution with rlnorm function in the stats R package. The *mean parameter* that defines this error distribution (i.e., the mean of the variable's natural logarithm) is equal to the log of the *median* age estimate of a given specimen (as estimated by the model fitting), and the variance (of the variable's natural logarithm) is equal to 0.056 (as estimated by the model fitting). The best model with the gamma distribution uncertainty for *C. gibba* is the simple power-law kinetics model

for Asp D/L (SPK0, with the scale corresponding to variance parameter equal to 4.784, and shape corresponding to median age estimated divided by variance). For *G. minima*, the best-supported calibration (based on 13 shells dated by ^{14}C and on two live collected shells) is represented by the simple power-law kinetics model (SPK0) for Asp D/L, with the initial D/L value set to zero (Fig. 4), and gamma uncertainty (with the scale corresponding to variance parameter equal to 51.16437, and shape corresponding to median age estimated divided by variance). The best model with the lognormal uncertainty is the TDK1 model for Asp D/L, with variance equal to 119.58. The estimates of variance from these four calibrations (two with lognormal and two with gamma uncertainty) can be used to model the effect of calibration error on the estimation of inter-quartile age range.

The component of time averaging expected due to the calibration error was computed by estimating an IQR for each shell expected under a repeated sampling of shell ages from lognormal and gamma distribution separately for both species. The mean IQR of all shells in a given increment represents the component of time averaging expected purely under calibration error. The time averaging corrected for this error refers to the difference between the raw IQR on one and the error component on the other hand (Dominguez *et al.*, 2016). However, simulations suggest that this approach tends to strongly underestimate the actual time averaging (M. Kowalewski, pers. comm., February 2022) and thus IQRs corrected for the AAR–^{14}C calibration error should be treated as minimum estimates.

Although the models based on lognormal and gamma uncertainty give similar estimates of central tendency (median age, see Tomašových et al., 2017 for *C. gibba* and Tomašových et al., 2019 for *G. minima*), they significantly differ in their estimate of age uncertainty. The variance increases quadratically with increasing age in calibrations with lognormal uncertainty, whereas it increases linearly with age in calibrations with gamma uncertainty (Allen et al., 2013). Consequently, the IQR corrected for the calibration age error can be very small when the lognormal uncertainty is used. For both species, the calibration based on the gamma uncertainty generates estimates of the corrected IQR that are around 1200 years, overlapping with the lower end of the raw estimates of IQR (Fig. S1). In contrast, the IQR corrected for calibration error is very small (<500 years) on the basis of lognormal uncertainty. Visual inspections of AAR-^{14}C calibrations for both species show that for shells older than ~500-1000 years, very broad 95% prediction intervals are predicted for lognormal uncertainty (exceeding beyond the calibration data), whereas 95% prediction intervals for shells of similar age are narrower for calibrations based on gamma uncertainty. The stronger support for the lognormal distribution for *C. gibba* probably reflects its more accurate estimation of ages for very young shells. Therefore, for assemblages with ages >1000 years, we presume that correcting IQR with the gamma uncertainty is more realistic than with the lognormal uncertainty.

Estimates of sedimentation rate and mixing depth

In the absence of disintegration and under steady-state input of dead skeletal remains, time averaging (IQR) can be approximated on the basis of net sediment accumulation rate and the depth of mixing, assuming that shells are buried and mixed independently as a natural logarithm of three divided by an inverse of burial time below the mixed layer. We estimated the net sedimentation rate and the depth of mixing by bioturbation based on downcore changes in median age of two bivalve species between the adjacent core increments (Fig. S3). We then compared the magnitude of time averaging expected from these parameters to the scale of time averaging observed in the shell bed.

Changes in post-mortem age distributions of the two bivalve species, *Corbula gibba* and *Gouldia minima,* were documented throughout the Piran 2 core by Tomašových et al. (2019). Here we present the combined age distributions (Fig. S3). The estimate of net sedimentation rate of the shell bed corresponds to the thickness of increments between adjacent dated levels divided by difference in median age. The approximate the depth of mixing is based on the vertical extent of homogeneity in median ages.

The downcore changes in median age of bivalve assemblages document very slow rates of sedimentation in the uppermost 30 cm (0.004-0.012 cm/yr), and a slight increase to 0.016-0.039 cm/y at 30-90 cm. The surface increments indicate that the present-day depth of the mixed layer (ML) is ~10 cm but subsurface age distributions show homogeneity in median age between 25 and 50 cm (Fig. S3). Depending on the thickness of the mixed layer, IQR of the shell bed is expected to vary between 1800 years (ML=10 cm), 3700 years (ML=20 cm), and 9200 years (ML=50 cm) (Fig. S3). The empirical IQRs of the eight taxa observed at 20-30 cm thus closely correspond to the value expected for net sedimentation rate (0.006 cm/yr) estimated for the subsurface shell bed. Moreover, the surface-subsurface transition in the shape of bivalve age distributions described by Tomašových et al. (2019) shows that in the present-day surface mixed layer valves older than 2000 years are sourced from the subsurface shell-bed increments where shells with this age have the highest abundance. These old shells (presently located almost at the sediment-water interface) are thus not constantly exposed in the taphonomic active zone but are rather temporally sequestered in the subsurface and occasionally exhumed upward. Therefore, exhumation of shells from the subsurface shell bed, where they are protected from bioerosion or aggressive pore waters, contributes to time averaging in the surface zone. Similar mechanism must have acted during the deposition of the shell bed leading to the extensive age-mixing observed in that interval.

References

Allen, A.P., Kosnik, M.A., and Kaufman, D.S., 2013, Characterizing the dynamics of amino acid racemization using time-dependent reaction kinetics: A Bayesian approach to fitting age-calibration models: Quaternary Geochronology, v. 18, p. 63–77, doi:10.1016/j.quageo.2013.06.003.

Crema, E.R., and Bevan, A., 2021, Inference from large sets of radiocarbon dates: Software and methods: Radiocarbon, v. 63, p. 23–39, doi:10.1017/RDC.2020.95.

Dominguez, J.G., Kosnik, M.A., Allen, A.P., Hua, Q., Jacob, D.E., Kaufman, D.S., and Whitacre, K., 2016, Time-averaging and stratigraphic resolution in death assemblages and Holocene deposits: Sydney Harbour's molluscan record: Palaios, v. 31, p. 564–575, doi:10.2110/palo.2015.087.

Heaton, T.J. et al., 2020, Marine20—the marine radiocarbon age calibration curve (0–55,000 cal B.P.): Radiocarbon, v. 62, p. 779–820, doi:10.1017/RDC.2020.68.

R Core Team, 2021, R: A Language and Environment for Statistical Computing. Version 4.1.2: Vienna, Austria, R Foundation for Statistical Computing, http://www. Rproject.org.

Siani, G., Paterne, M., Michel, E., Sulpizio, R., Sbrana, A., Arnold, M., and Haddad, G., 2001, Mediterranean sea surface radiocarbon reservoir age changes since the Last Glacial Maximum: Science, v. 294, p. 1917–1920, doi:10.1126/science.1063649.

Tomašových, A., Gallmetzer, I., Haselmair, A., Kaufman, D.S., Vidović, J., and Zuschin, M., 2017, Stratigraphic unmixing reveals repeated hypoxia events over the past 500 yr in the northern Adriatic Sea: Geology, v. 45, p. 363–366, doi:10.1130/G38676.1.

Tomašových, A., Gallmetzer, I., Haselmair, A., Kaufman, D.S., Mavrič, B., and Zuschin, M., 2019, A decline in molluscan carbonate production driven by the loss of vegetated habitats encoded in the Holocene sedimentary record of the Gulf of Trieste: Sedimentology, v. 66, p. 781–807, doi:https://doi.org/10.1111/sed.12516.

TABLE S1. SIZE (LARGEST DIMENSION), MASS AND MINERALOGY OF THE DATED SKELETAL ELEMENTS, AND LIFE HABITS OF THEIR PRODUCERS

Taxon	Taxonomic affiliation	*N**	Skeletal element	Mineralogy	Mean mass (mg)	Mass range (mg)	Mean size (mm)	Size range (mm)	Life habit
Corbula gibba	Bivalvia	25	Shell	Aragonite	N.D.†	N.D.	4.25	3.19–5.84	Infaunal filter feeder
Gouldia minima	Bivalvia	30	Shell	Aragonite	N.D.	N.D.	3.74	2.09–8.27	Infaunal filter feeder
Adelosina intricata	Foraminifera	40	Test	High-Mg calcite	1.25	0.7–2.3	1.88	1.57–2.31	Epifaunal omnivore
Elphidium crispum	Foraminifera	40	Test	Low-Mg calcite	1.21	0.5–3	1.7	1.36–2.41	Epifaunal omnivore
Echinocyamus pusillus	Echinoidea	25	Test	High-Mg calcite	2.68	0.5–8.1	2.72	1.6–4.84	Infaunal deposit feeder
Psammechinus/ Paracentrotus	Echinoidea	14	Madreporite	High-Mg calcite	2.01	0.5–4.5	2.10	1.28–2.73	Epifaunal grazer
Pilumnus sp.	Brachyura	17	Chelae	Low-Mg calcite	11.38	1.6–70.4	4.64	2.99–9.29	Epifaunal carnivore
Gobius niger	Teleostei	16	Otolith	Aragonite	5.97	1.3–16.8	2.61	1.55–4.18	Nektobenthic carnivore

**N* —number of dated specimens
†N.D. —no data available

TABLE S2. *P*-VALUES FOR THE PAIRWISE WILCOXON TEST WITH A-POSTERIORI HOLM'S CORRECTION

	Corbula gibba	*Gouldia minima*	*Adelosina intricata*	*Elphidium crispum*	*Echinocyamus pusillus*	*Psammechinus/ Paracentrotus*	*Pilumnus sp.*
Gouldia minima	**<0.001**	NA	NA	NA	NA	NA	NA
Adelosina intricata	1	**0.002**	NA	NA	NA	NA	NA
Elphidium crispum	**<0.001**	1	**<0.001**	NA	NA	NA	NA
Echinocyamus pusillus	1	1	0.116	0.288	NA	NA	NA
Psammechinus/ Paracentrotus	0.253	1	0.165	1	1	NA	NA
Pilumnus sp.	1	0.674	1	0.081	1	1	NA
Gobius cobitis	1	1	0.651	0.414	1	1	1

Note: significant differences in median age are marked in bold

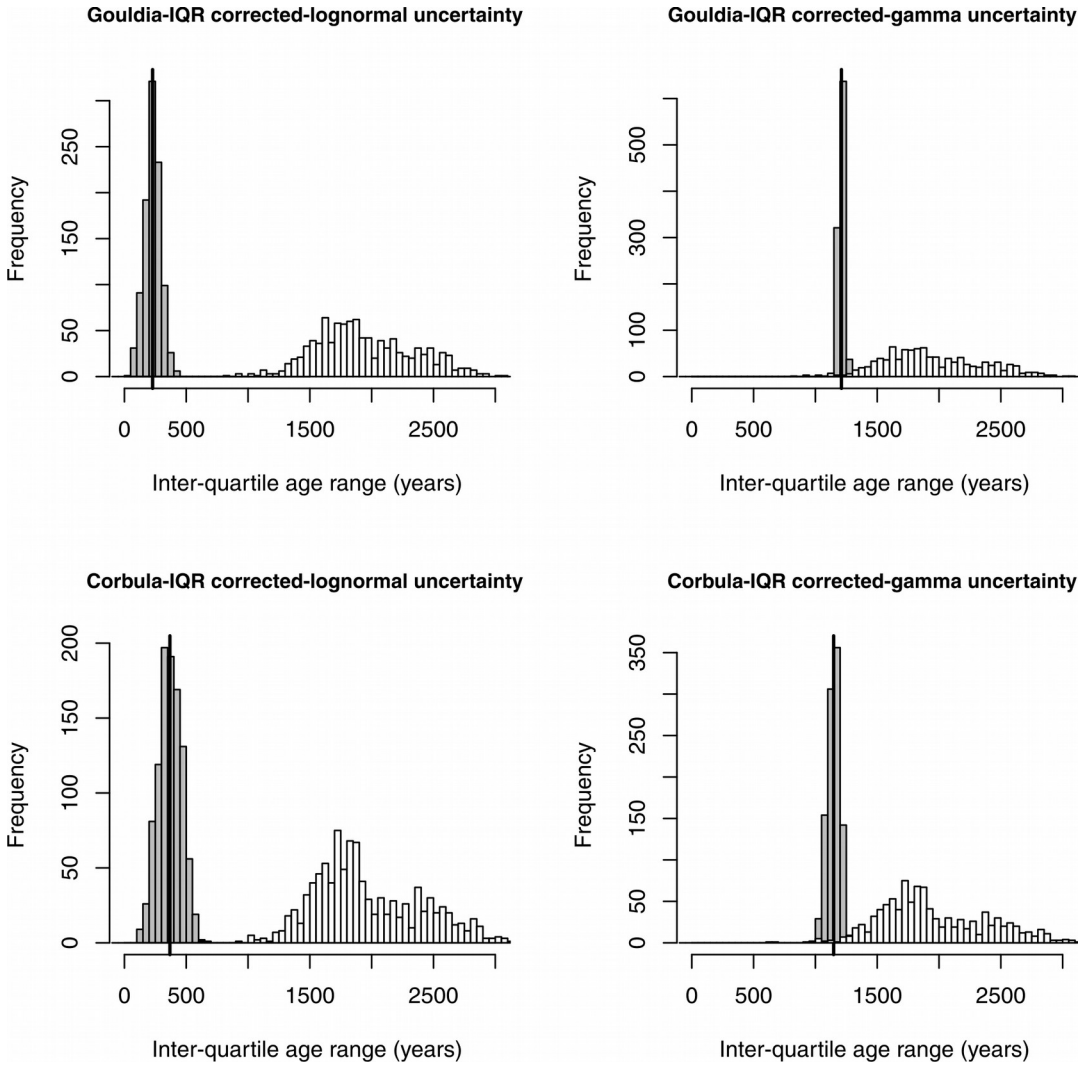

Figure S1. Effect of the correction for the AAR–^{14}C calibration error on the IQR estimates. White distribution represent the empirical bootstrapped IQR. The gray distributions represent the IQR corrected for calibration age error. The corrected values provide the end-member minimum estimate of the scale of time averaging in the two bivalve species.

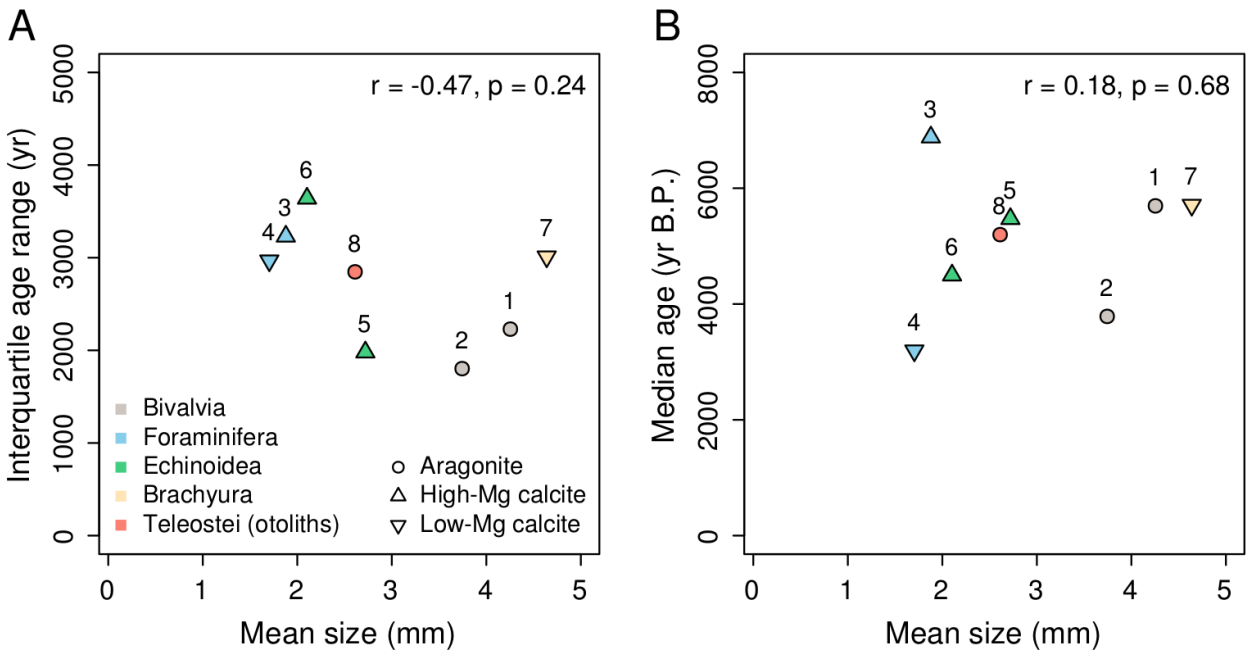

Figure S2. Mean size (the largest dimension) of the dated skeletal elements versus their (A) interquartile age range and (B) median age. 1: *Corbula gibba*, 2: *Gouldia minima*, 3: *Adelosina intricata*, 4: *Elphidium crispum*, 5: *Echinocyamus pusillus*, 6: *Psammechinus/Paracentrotus*, 7: *Pilumnus sp.*, 8: *Gobius niger*.

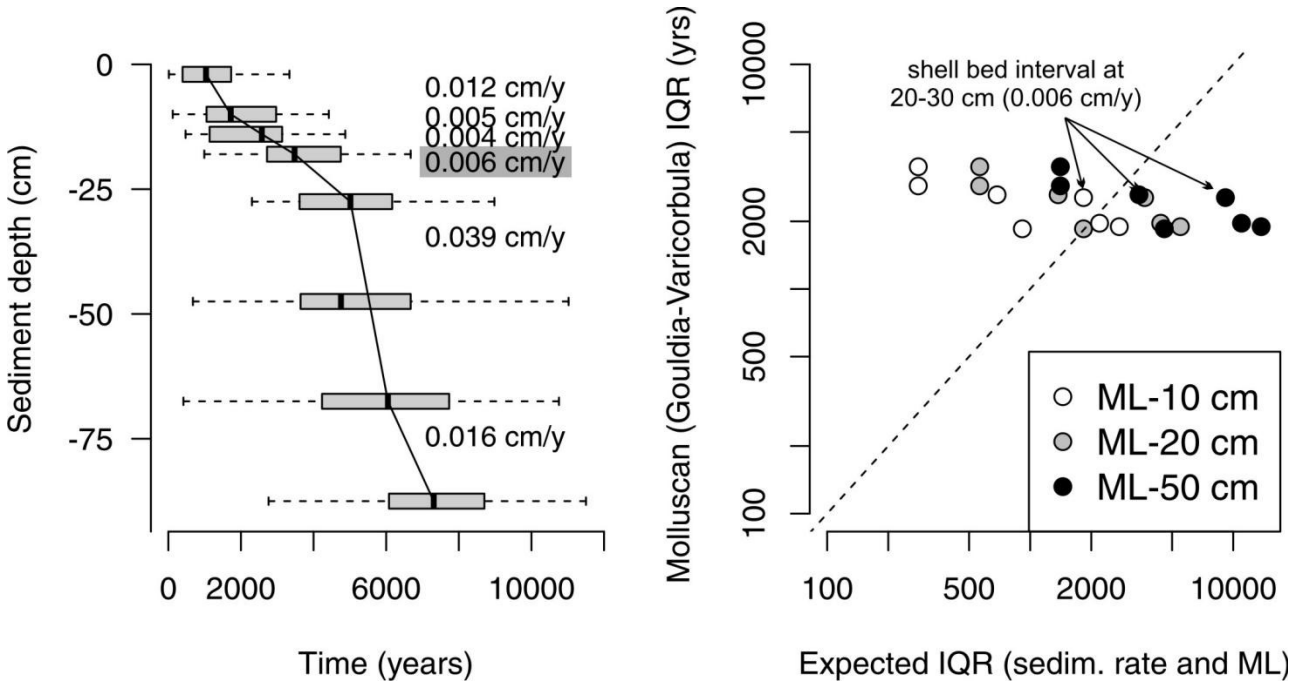

Figure S3. Left: Estimates of net sedimentation rate based on the downcore changes in median shell age at Piran (data from Tomašových et al., 2019). The interval at 20-30 cm indicates the long-term deposition rate of about ~0.006 cm/yr (dark-shaded estimate). Right: Time averaging of pooled *Gouldia minima* and *Corbula gibba* assemblage at each stratigraphic level is contrasted with the expected IQR based on the corresponding sedimentation rate (here, the rate that characterizes the immediate overlie of the increment) and three estimates of the depth of the mixed layer (10, 20 and 50 cm). The arrows point to the estimates for the shell bed interval. This relationship shows that the observed time averaging is congruent with the estimates expected under mixing depth equal to 10 or 20 cm. The IQR of the bivalve assemblage at 25-30 cm is equal to 2550 years.

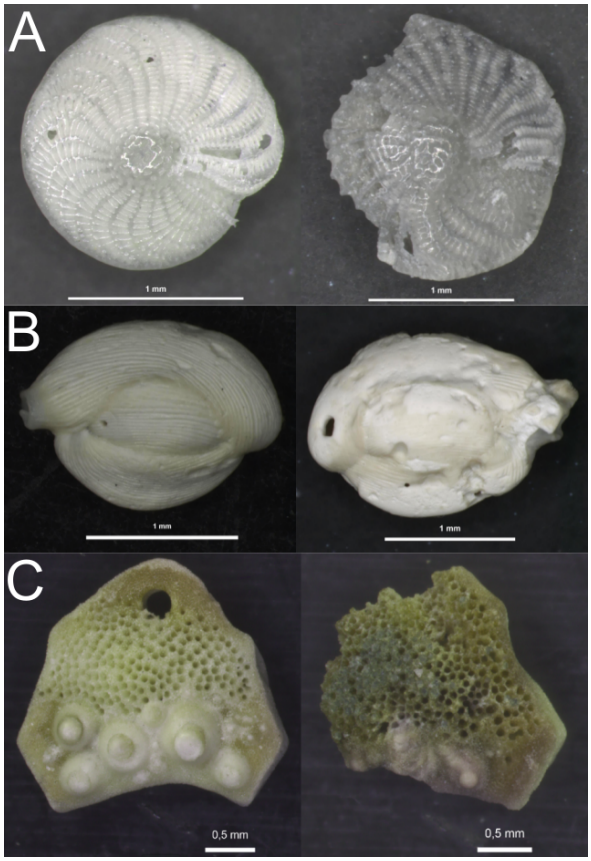

Figure S4. Examples of radiocarbon-dated skeletal elements showing different degree of taphonomic alteration: (A) tests of *Elphidium crispum* (calibrated age of the specimens: 1445 and 3213 yr B.P.), (B) tests of *Adelosina intricata* (age of the specimens: 3587 and 7459 yr B.P.), and (C) madreporites of *Psammechinus/Paracentrotus* (age of the specimens: 7450 and 6968 yr B.P.).